Ultracold Rare-Earth Magnetic Atoms with an Electric Dipole Moment

Maxence Lepers, Hui Li, Jean-François Wyart, Goulven Quéméner, Olivier Dulieu

Ultracold rare-earth magnetic atoms with an electric dipole moment

Maxence Lepers[1,2], Hui Li[1], Jean-François Wyart[1,3], Goulven Quéméner[1] and Olivier Dulieu[1]
[1] *Laboratoire Aimé Cotton, CNRS, Université Paris-Sud, ENS Paris-Saclay, Université Paris-Saclay, 91405 Orsay, France*
[2] *Laboratoire Interdisciplinaire Carnot de Bourgogne, CNRS, Université de Bourgogne Franche-Comté, 21078 Dijon, France* and*
[3] *LERMA, Observatoire de Paris-Meudon, PSL Research University, Sorbonne Universités, UPMC Univ. Paris 6, CNRS UMR8112, 92195 Meudon, France*
(Dated: September 11, 2018)

We propose a new method to produce an electric and magnetic dipolar gas of ultracold dysprosium atoms. The pair of nearly degenerate energy levels of opposite parity, at 17513.33 cm^{-1} with electronic angular momentum $J = 10$, and at 17514.50 cm^{-1} with $J = 9$, can be mixed with an external electric field, thus inducing an electric dipole moment in the laboratory frame. For field amplitudes relevant to current-day experiments, *i.e.* an electric field of 5 kV/cm, we predict a large magnetic dipole moment up to 13 Bohr magnetons, and sizeable electric dipole moment up to 0.22 debye. When a magnetic field is present, we show that the induced electric dipole moment is strongly dependent on the angle between the fields. The lifetime of the field-mixed levels is found in the millisecond range, thus allowing for suitable experimental detection and manipulation.

Introduction. In a classical neutral charge distribution, a dipole moment appears with a separation between the barycenter of positive and negative charges [1]. An obvious example is provided by an heteronuclear diatomic molecule, which possesses a permanent dipole moment along its interatomic axis. It will manifest in the laboratory frame when such a molecule is placed in an external electric field, acquiring a preferred orientation along the direction of the field. Moreover, a neutral atom placed in an external electric field acquires a small dipole moment, as the spherical symmetry of space is broken. This effect is spectacularly maximized in Rydberg atoms, where the maximal induced dipole moment scales as n^2, where n is the principal quantum number of the considered Rydberg state [2].

At the single-particle scale, the external electric field mixes even and odd-parity levels of the energy spectrum: rotational levels for a diatomic molecule (see *e.g.* [3]), or levels with different orbital angular momenta for Rydberg atoms (see *e.g.* [4]). In both cases, this leads to a pronounced linear Stark shift on the energy levels, revealing the existence of a permanent dipole moment in the laboratory frame. More suprisingly, it has been observed that a homonuclear diatomic molecule formed by a Rydberg atom bound to a ground state atom located inside the Rydberg electron orbital, can exhibit a permanent electric dipole moment in the laboratory frame [5, 6].

The search for such dipolar systems, involving especially lanthanide atoms, is currently very active in the context of ultracold dilute gases [7–18]. Indeed, the particles of the gas interact through a highly anisotropic long-range potential energy varying as the inverse cubic power of their spatial separation [19, 20]. Prospects related to many-body physics, quantum simulation and ultracold chemistry are nowadays within reach experimentally [21–23]. A particular attention is paid to gases with an electric and a magnetic dipole moment, which up to now consist of paramagnetic polar diatomics [24–33].

In dysprosium (Dy), there exists a pair of quasi-degenerate opposite-parity levels at 19797.96 cm^{-1}, split by less than 0.01 cm^{-1}, possessing the same electronic angular momentum $J = 10$, and which have been employed for fundamental measurements [34–40]. However, the reduced transition dipole moment (TDM) coupling those two levels, equal to 0.038 D [35] (1 D = 0.393456 ea_0, e being the unsigned electron charge and a_0 the Bohr radius), is not sufficient to observe dipolar effects. On the contrary, we demonstrate in the present work, that the odd-parity level $|a\rangle$ at $E_a = 17513.33$ cm^{-1} with $J_a = 10$ and main configuration [Xe]$4f^{10}6s6p$ ([Xe] being the xenon core), and the even-parity level $|b\rangle$ at $E_b = 17514.50$ cm^{-1} with $J_b = 9$ and main configuration [Xe]$4f^{10}5d6s$ [41], which present a reduced TDM of 8.16 D, are promising candidates to produce an electric and magnetic dipolar gas of ultracold atoms.

In this Letter, we set up the effective Hamiltonian for the two opposite-parity excited levels $|a\rangle$ and $|b\rangle$ in the presence of electric and magnetic fields with arbitrary relative orientation. We use energies and g-factors from Ref. [42], and TDMs and radiative lifetimes based on our own well-established semi-empirical electronic-structure calculations. For an experimentally accessible electric field of 5 kV/cm and magnetic field of 100 G, we predict a field-mixed level with a permanent magnetic dipole moment (PMDM) of $\mu^* = 13\ \mu_B$ (with μ_B the Bohr magneton), to our knowledge the largest value observed in ultracold experiments, and an induced electric dipole moment (IEDM) of $d^* = 0.22$ D, which is similar to the value obtained in the pioneering experiment on KRb [43]. We demonstrate a strong control of the IEDM, which ranges from 0 to d^* as a function of the angle between the fields. We also calculate the atomic radiative lifetime as functions of the fields parameters, and obtain a few milliseconds for the level characterized by μ^* and d^*.

Finally, we show that our method is applicable for all bosonic and fermionic isotopes of Dy.

Model. We consider an atom in two energy levels $|a\rangle$ and $|b\rangle$, of energies E_i and total angular momentum J_i ($i = a, b$). Here $E_a = 17513.33$ cm^{-1}, $J_a = 10$ and $E_b = 17514.50$ cm^{-1}, $J_b = 9$ [42]. Firstly, we consider bosonic isotopes which have no nuclear spin, $I = 0$. In absence of field, each level $|i\rangle$ is $(2J_i + 1)$-time degenerate, and the corresponding Zeeman subslevels are labeled with their magnetic quantum number M_i. The atom is submitted both to a magnetic field $\mathbf{B} = B\mathbf{e}_z$, with $\mathbf{e}_z$ the unit vector in the z direction, taken as quantization axis, and to electric field $\mathbf{E} = \mathcal{E}\mathbf{u}$, with $\mathbf{u}$ a unit vector in the direction given by the polar angles θ and $\phi = 0$. In the basis $\{|M_a = -J_a\rangle, ..., |+J_a\rangle, |M_b = -J_b\rangle, ..., |+J_b\rangle\}$ spanned by the Zeeman sublevels of $|a\rangle$ and $|b\rangle$, the Hamiltonian can be written

$$\hat{H} = \sum_{i=a,b} E_i \sum_{M_i=-J_i}^{J_i} |M_i\rangle\langle M_i| + \hat{W}_Z + \hat{W}_S \,. \qquad (1)$$

The Zeeman Hamiltonian $\hat{W}_Z$ only contains diagonal terms equal to $M_i g_i \mu_B B$, with $g_a = 1.30$ and $g_b = 1.32$ the Landé g-factors [42]. The last term of Eq. (1) is the Stark Hamiltonian, which couples sublevels $|M_a\rangle$ with sublevels $|M_b\rangle$ as

$$\langle M_a|\hat{W}_S|M_b\rangle = -\sqrt{\frac{4\pi}{3(2J_a+1)}}\langle a\|\hat{\mathbf{d}}\|b\rangle\,\mathcal{E} \times Y^*_{1,M_a-M_b}(\theta,0)\, C^{J_a M_a}_{J_b M_b,1,M_a-M_b} \,, \qquad (2)$$

where $\langle a\|\hat{\mathbf{d}}\|b\rangle$ is the reduced TDM, $Y_{kq}(\theta,\phi)$ a spherical harmonics and $C^{c\gamma}_{a\alpha b\beta}$ a Clebsch-Gordan coefficient [44]. For given values of $\mathcal{E}$, B and θ, we calculate the eigenvalues E_n and eigenvectors

$$|\Psi_n\rangle = \sum_{i=a,b} \sum_{M_i=-J_i}^{J_i} c_{n,M_i}|M_i\rangle \qquad (3)$$

of the Hamiltonian in Eq. (1).

The reduced TDM $\langle a\|\hat{\mathbf{d}}\|b\rangle$ and the natural line widths γ_i are calculated using the method developed in our previous works [45–48], based on the least-square fitting procedure of energies present in the Cowan codes [49], and extended by us to Einstein coefficients. Firstly, odd-level energies are taken from Ref. [47] which include the electronic configurations [Xe]$4f^{10}6s6p$ and [Xe]$4f^9 5d6s^2$. Even-level energies are calculated with the configurations [Xe]$4f^{10}6s^2$, [Xe]$4f^{10}5d6s$ and [Xe]$4f^9 6s^2 6p$ [50]. Secondly, following Ref. [47], we adjust the mono-electronic TDMs by multiplying their *ab initio* values by appropriate scaling factors [46], equal to 0.794 for $\langle 6s|\hat{r}|6p\rangle$, 0.923 for $\langle 4f|\hat{r}|5d\rangle$ and 0.80 for $\langle 5d|\hat{r}|6p\rangle$ [51]. From the resulting Einstein coefficients, we can extract $\langle a\|\hat{\mathbf{d}}\|b\rangle = 3.21$ a.u., as well as the natural linewidth $\gamma_b = 2.98 \times 10^4$ s^{-1}, resulting from decays to levels of the [Xe]$4f^{10}6s6p$ configuration. At the electric-dipole approximation, γ_a vanishes; considering electric-quadrupole and magnetic-dipole transitions, especially towards the level [Xe]$4f^{10}(^5I_8).6s6p(^3P^o_1)\,(8,1)^o_9$ at 15972.35 cm^{-1}, it can be estimated with the Cowan codes [49] as $\gamma_a = 3.56 \times 10^{-2}$ s^{-1}.

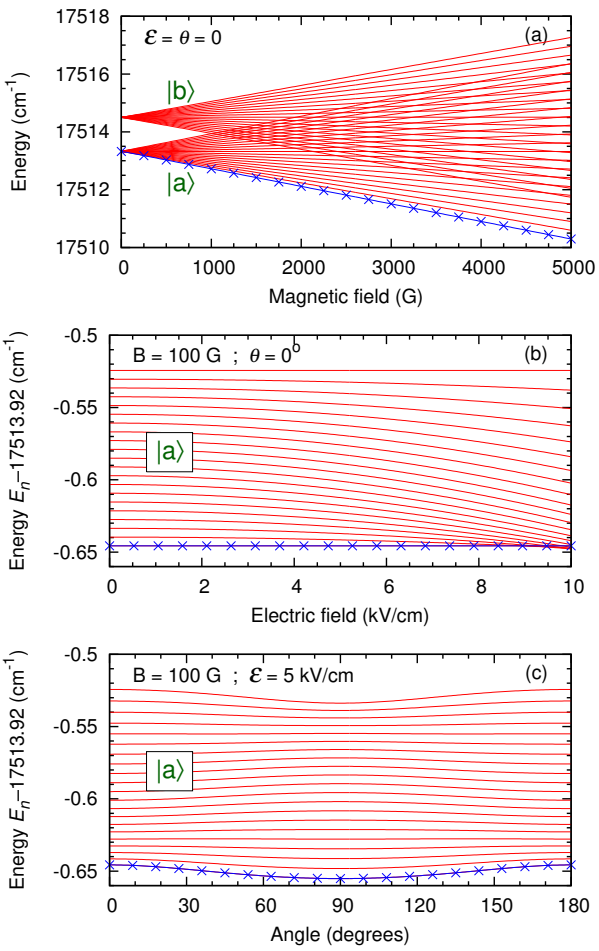

FIG. 1. Eigenvalues of the atom-field Hamiltonian (1) as functions of: (a) the magnetic field B for vanishing electric field and angle $\mathcal{E} = \theta = 0$; (b) the electric field $\mathcal{E}$ for $B = 100$ G and $\theta = 0°$; (c) the angle θ for $B = 100$ G and $\mathcal{E} = 5$ kV/cm. In panels (b) and (c), the origin of energies is taken at $(E_a + E_b)/2 = 17513.92$ cm^{-1}. The blue curve with crosses corresponds to the eigenstate converging towards $|M_a = -10\rangle$ when $\theta \to 0$.

Energies in electric and magnetic fields. Figure 1(a) shows the eigenvalues of the Hamiltonian (1) as functions of the magnetic field for $\mathcal{E} = \theta = 0$. The field splits levels $|a\rangle$ and $|b\rangle$ into 21 and 19 sublevels respectively, each one associated with a given M_a or M_b; from now on, we emphasize the lowest sublevel $|M_a = -10\rangle$. Due to the close Landé g-factors, the two Zeeman manifolds look very similar, *i.e.* the branches characterized by the same values $M_a = M_b$ are almost parallel. For $B \geq 1000$

gauss, the two Zeeman manifolds overlap; but because the magnetic field conserves parity, the sublevels of $|a\rangle$ and $|b\rangle$ are not mixed. Provoking that mixing is the role of the electric field.

On figure 1(b), we plot the 21 lowest eigenvalues of Eq. (1) as functions of the electric field for $B = 100$ gauss and $\theta = 0°$. We focus on the eigenstates converging to the sublevels of $|a\rangle$ when $\mathcal{E} \to 0$. In the range of field amplitudes chosen in Figs. 1(a) and (b), which corresponds to current experimental possibilities, the influence of $\mathcal{E}$ is much weaker than the influence of B. On Fig. 1(b), the energies decrease quadratically with the electric field, because the sublevels of $|a\rangle$ are repelled by the sublevels of $|b\rangle$. Since $\theta = 0°$, the z component of the total angular momentum is conserved, and so, the sublevels for which $M_a = M_b$ are coupled in pairs. In consequence, the sublevels $|M_a = \pm 10\rangle$ are insensitive to the electric field, as they have no counterparts among the sublevels of $|b\rangle$ (recalling that $J_b = 9$).

The only way to couple the $|M_a = \pm 10\rangle$ sublevels to the other ones is to rotate, say, the electric field, and thus break the cylindrical symmetry around the z axis. On figure 1(c), the 21 lowest eigenvalues of Eq. (1) are now shown as function of the angle θ, for fixed field amplitudes, $\mathcal{E} = 5$ kV/cm and $B = 100$ gauss. Even if the corresponding eigenvectors are not associated with a single sublevel $|M_i\rangle$ (unlike Figs. 1(a) and (b)), they can conveniently be labeled $|\overline{M}_i\rangle$ after their field-free or $\theta = 0$ counterparts. For a given eigenstate, the θ-dependence of energy is weak. However for $|\overline{M}_a = \pm 10\rangle$, the energy decrease reveals the repulsion with sublevels of $|b\rangle$, which is maximum for $\theta = 90°$.

Permanent magnetic and induced electric dipole moments. The z component of the PMDM associated with the eigenvector $|\Psi_n\rangle$ is equal to

$$\mu_n = -\mu_B \sum_{i=a,b} g_i \sum_{M_i=-J_i}^{J_i} |c_{n,M_i}|^2 M_i. \qquad (4)$$

Since the eigenvectors are mostly determined by their field-free counterparts, μ_n does not change significantly in our range of field amplitudes; it is approximately equal to $\mu_n \approx -\overline{M}_a g_a \mu_B$ for $n \in [1; 21]$ and $\mu_n \approx -\overline{M}_b g_b \mu_B$ for $n \in [22; 40]$. For instance, the state $|\overline{M}_a = -10\rangle$ has the maximal value $\mu^* = 13.0 \times \mu_B$.

The mean IEDM $d_n = \langle \Psi_n | \mathbf{d} \cdot \mathbf{u} | \Psi_n \rangle$ associated with the eigenvector $|\Psi_n\rangle$ in the direction $\mathbf{u}$ of the electric field is

$$d_n = -\frac{1}{\mathcal{E}} \sum_{M_a,M_b} c^*_{n,M_a} c_{n,M_b} \langle M_a | \hat{W}_S | M_b \rangle + c.c., \qquad (5)$$

where the matrix element of $\hat{W}_S$ is given in Eq. (2). Figure 2(a) presents the IEDMs as functions of the electric field $\mathcal{E}$, for $B = 100$ G and $\theta = 0°$. In this case, the graph is symmetric about the y axis. All the curves increase linearly with $\mathcal{E}$; all, except the lowest and highest ones, correspond to two eigenstates. In agreement with Fig. 1(b), the curve $d_n = 0$ is associated with $|\overline{M}_a = \pm 10\rangle$ ($n = 1$ and 21). The lowest and highest curves belong to $\overline{M}_{a,b} = 0$, for which by contrast, the PMDM vanishes.

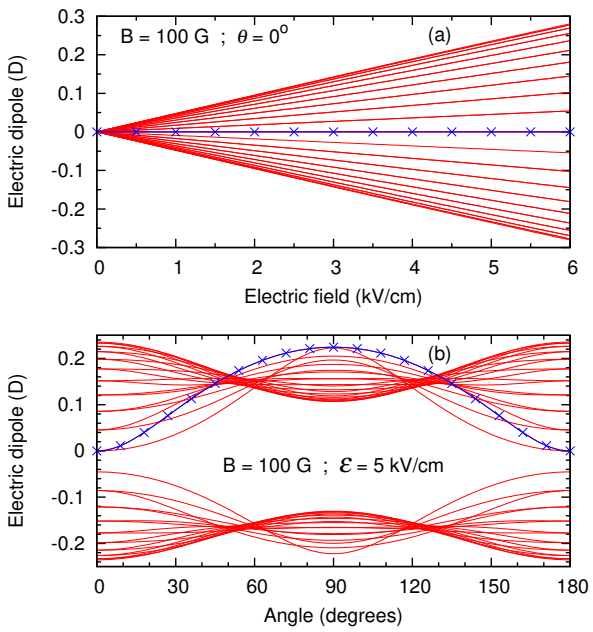

FIG. 2. Induced electric dipole moments, see Eq. (5), associated with the eigenstates of the atom-field Hamiltonian (1) as functions of: (a) the electric field $\mathcal{E}$ for $B = 100$ G and $\theta = 0°$; (b) the angle θ for $B = 100$ G and $\mathcal{E} = 5$ kV/cm. The blue curve with crosses corresponds to the eigenstate $|\overline{M}_a = -10\rangle$.

As shows figure 2(b), the IEDMs change dramatically as functions of the angle θ. In particular, the IEDM of the eigenstate $|\overline{M}_a = -10\rangle$ ranges continuously from 0 to a maximum $d^* = 0.224$ D for $\theta = 90°$. The eigenstate $|\overline{M}_a = 10\rangle$ follows a similar evolution, except that its curve is sharper around its maximum. In contrast, the IEDM of the eigenstate $|\overline{M}_a = 0\rangle$, which is the largest for $\theta = 0°$, becomes the smallest for 90°. Compared to the eigenstates $|\overline{M}_a\rangle$, the curves corresponding to the eigenstates $|\overline{M}_b\rangle$ exhibit an approximate reflection symmetry around the y axis. Finally, it is important to mention that the influence of the magnetic field on the IEDMs is weak in the amplitude range of Fig. 1(a).

Radiative lifetimes. The radiative lifetime $\tau_n = 1/\gamma_n$ associated with eigenvector $|\Psi_n\rangle$ is such that γ_n is an arithmetic average of the natural line widths of $|a\rangle$ and $|b\rangle$,

$$\tau_n = \gamma_n^{-1} = \left(\sum_{i=a,b} \gamma_i \sum_{M_i=-J_i}^{J_i} |c_{n,M_i}|^2 \right)^{-1}. \qquad (6)$$

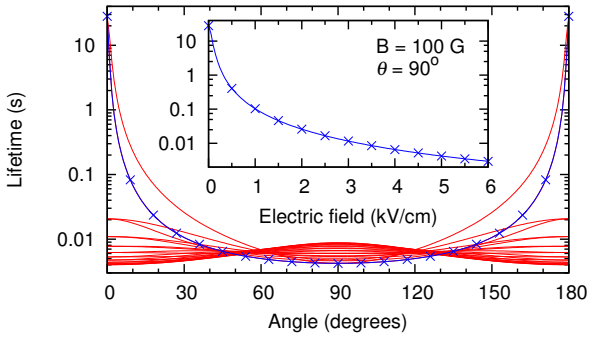

FIG. 3. Radiative lifetimes, see Eq. (6), associated with the eigenstates $|\overline{M}_a\rangle$ as functions of the angle θ for $B = 100$ G and $\mathcal{E} = 5$ kV/cm. The blue curve with crosses corresponds to the eigenstate $|\overline{M}_a = -10\rangle$. The inset shows the lifetime of this eigenstate as a function of $\mathcal{E}$ for $B = 100$ G and $\theta = 90°$.

Figure 3 displays the lifetimes of all eigenstates of Eq. (1) as functions of the angle θ for $\mathcal{E} = 5$ kV/cm and $B = 100$ G. Because the natural line widths γ_a and γ_b differ by 6 orders of magnitude, the lifetimes τ_n are also spread over a similar range. At the field amplitudes of Fig. 3, the eigenvectors $|\overline{M}_a\rangle$ are composed at least of 90 % of sublevels of $|a\rangle$, and similarly for eigenstates $|\overline{M}_b\rangle$. Therefore, the lifetimes of eigenstates $|\overline{M}_b\rangle$ (not shown on Fig. 3) are approximately $1/\gamma_b$, and they weakly depend on θ. As for the eigenstates $|\overline{M}_a\rangle$, their small $|b\rangle$ components, say ε, induces lifetimes roughly equal to $\approx \tau_b/\varepsilon^2$. For $|\overline{M}_a = \pm 10\rangle$, the lifetime ranges from $\tau^* = 4.22$ ms for $\theta = 90°$ to $\tau_a = 28.1$ s for $\theta = 0°$. Again, this illustrates that the coupling with the sublevels of $|b\rangle$ is maximum for perpendicular fields and absent for colinear ones.

The inset of figure 3 shows the lifetime of the eigenstate $|\overline{M}_a = -10\rangle$ as function of $\mathcal{E}$. In this range of field amplitude, τ_1 scales as $\mathcal{E}^{-2}$. So, a large amplitude $\mathcal{E}$ can strongly affect the lifetime of the atoms; but on the other hand, $\mathcal{E}$ needs to be sufficient to generate a sizeable IEDM. So, there is a compromise to find between IEDM and lifetime, by tuning the electric-field amplitude and the angle between the fields.

Fermionic isotopes. There are two fermionic isotopes of dysprosium, ^{161}Dy and ^{163}Dy, both with a nuclear spin $I = 5/2$. A given hyperfine sublevel is characterized by the total (electronic+nuclear) angular momentum F_i and its z-projection M_{F_i}, where $|J_i - I| \leq F_i \leq J_i + I$, and $-F_i \leq M_{F_i} \leq F_i$. Namely, F_a ranges from 15/2 to 25/2, and F_b ranges from 13/2 to 23/2. The hyperfine sublevels are constructed by angular-momentum addition of $\mathbf{J}_i$ and $\mathbf{I}$, *i.e.* $|F_i M_{F_i}\rangle = \sum_{M_i M_I} C^{F_i M_{F_i}}_{J_i M_i I M_I} |J_i M_i\rangle |I M_I\rangle$. Compared to Eq. (1), the Hamiltonian $\hat{H}'$ is modified as

$$\hat{H}' = \sum_{i=a,b} \sum_{F_i} E_{F_i} \sum_{M_{F_i}} |F_i M_{F_i}\rangle\langle F_i M_{F_i}| + \hat{W}_Z + \hat{W}_S \quad (7)$$

TABLE I. Maximal induced electric dipole moment d^*, dipolar length a_d [54] and minimal lifetime τ^* obtained for different isotopes of dysprosium for an electric field $\mathcal{E} = 5$ kV/cm, a magnetic field $B = 100$ G and an angle $\theta = 90°$. The results of ^{162}Dy are also valid for the other bosonic isotopes ^{156}Dy, ^{158}Dy, ^{160}Dy and ^{164}Dy.

	d^* (D)	a_d (a_0)	τ^* (ms)
^{161}Dy	0.225	2299	4.18
^{162}Dy	0.224	2293	4.22
^{163}Dy	0.222	2266	4.23

where E_{F_i} is the hyperfine energy depending on the magnetic-dipole and electric-quadrupole constants A_i and B_i. For ^{163}Dy, they have been calculated in Ref. [52]: $A_a = 225$ MHz, $B_a = 2434$ MHz, $A_b = 237$ MHz and $B_b = 706$ MHz. For ^{161}Dy, we apply the relations $(^{161}A_i) = -0.714 \times (^{163}A_i)$ and $(^{161}B_i) = 0.947 \times (^{163}B_i)$ given in Ref. [53]. The matrix elements of the Zeeman $\hat{W}_Z$ and Stark Hamiltonians $\hat{W}_S$ are calculated by assuming that they do not act on the nuclear quantum number M_I, and by using the formulas without hyperfine structure (see Eq. (2) and text above).

After diagonalizing Eq. (7), one obtains 240 eigenstates (compared to 40 in the bosonic case). Despite their large number of curves, the plots of energies, IEDMs and lifetimes show similar features to figures 1–3. The eignestates $|\Psi'_n\rangle$ can be labeled $|\overline{F}_i \overline{M}_{F_i}\rangle$ after their field-free counterparts $|F_i M_{F_i}\rangle$. Moreover, the "stretched" eigenstates $|\overline{F}_a \overline{M}_{F_a}\rangle = |25/2, \pm 25/2\rangle$ are not sensitive to the electric field for $\theta = 0°$, and maximally coupled for $\theta = 90°$; and so, their IEDMs range from 0 up to d^* and their lifetimes from τ_a down to τ^*. As shows Table I, for the same field characteristics, the values of d^* and τ^* are very similar from one isotope to another.

Table I also contains the so-called dipolar length $a_\mathrm{d} = m(d^*/\hbar)^2$ [54]. It characterizes the length at and beyond which the dipole-dipole interaction between two particles is dominant. For the ^{161}Dy isotope, one can reach a dipolar length of $a_\mathrm{d} = 2299\ a_0$. To compare with, at $\mathcal{E} = 5$ kV/cm and an IEDM of 0.22 D [43], ^{40}K^{87}Rb has a length of $a_\mathrm{d} = 1734\ a_0$. Similarly, a length of $a_\mathrm{d} = 1150\ a_0$ was reached [11] for magnetic dipolar Feshbach molecules of ^{168}Er$_2$. Therefore one can obtain comparable and even stronger dipolar character with excited Dy atoms than with certain diatomics. However, the collisions are likely to affect the sample lifetime, unless the atoms are loaded in an optical lattice.

Conclusion. We have demonstrated the possibility to induce a sizeable electric dipole moment on atomic dysprosium, in addition to its large magnetic dipole moment. To do so, the atoms should be prepared in a superposition of nearly degenerate excited levels using an electric and a magnetic field of arbitrary orientations. We show a remarkable control of the induced electric dipole mo-

ment and radiative lifetime by tuning the angle between the fields. Being metastable, those two levels are not accessible by one-photon transition from the ground level. Instead, one could perform a two-photon transition to a high-lying even-parity level and then rely on spontaneous emission towards $|a\rangle$ [35], or a Raman transition between the ground level $|g\rangle$ ($J_g = 8$) and the level $|b\rangle$ ($J_b = 9$), through the upper levels at 23736.61, 23832.06 or 23877.74 cm^{-1}, whose $[Xe]4f^{10}6s6p$ character insures significant transition strengths with $|g\rangle$ and $|b\rangle$. In the spectrum of other lanthanides, there exist pairs of quasi-degenerate levels accessible from the ground state, for instance the levels at 24357.90 and 24660.80 cm^{-1} in holmium, but in turn their radiative lifetime is much shorter [55].

Acknowledgments. We acknowledge support from "DIM Nano-K" under the project "InterDy", and from "Agence Nationale de la Recherche" (ANR) under the project "COPOMOL" (contract ANR-13-IS04-0004-01). We also acknowledge the use of the computing center "MésoLUM" of the LUMAT research federation (FR LUMAT 2764).

* maxence.lepers@u-bourgogne.fr

[1] J. Jackson, *Classical Electrodynamics* (John Wiley & Sons, Inc., New York, 1999).
[2] T. Gallagher, *Rydberg atoms*, Vol. 3 (Cambridge University Press, 2005).
[3] M. Brieger, Chem. Phys. **89**, 275 (1984).
[4] M. Zimmerman, M. Littman, M. Kash, and D. Kleppner, Phys. Rev. A **20**, 2251 (1979).
[5] C. Greene, A. Dickinson, and H. Sadeghpour, Phys. Rev. Lett. **85**, 2458 (2000).
[6] W. Li, T. Pohl, J. Rost, S. Rittenhouse, H. Sadeghpour, J. Nipper, B. Butscher, J. B. Balewski, V. Bendkowsky, R. Löw, and T. Pfau, Science **334**, 1110 (2011).
[7] M. Lu, S. Youn, and B. Lev, Phys. Rev. Lett. **104**, 063001 (2010).
[8] D. Sukachev, A. Sokolov, K. Chebakov, A. Akimov, S. Kanorsky, N. Kolachevsky, and V. Sorokin, Phys. Rev. A **82**, 011405 (2010).
[9] K. Aikawa, A. Frisch, M. Mark, S. Baier, A. Rietzler, R. Grimm, and F. Ferlaino, Phys. Rev. Lett. **108**, 210401 (2012).
[10] J. Miao, J. Hostetter, G. Stratis, and M. Saffman, Phys. Rev. A **89**, 041401 (2014).
[11] A. Frisch, M. Mark, K. Aikawa, S. Baier, R. Grimm, A. Petrov, S. Kotochigova, G. Quéméner, M. Lepers, O. Dulieu, and F. Ferlaino, Phys. Rev. Lett. **115**, 203201 (2015).
[12] H. Kadau, M. Schmitt, M. Wenzel, C. Wink, T. Maier, I. Ferrier-Barbut, and T. Pfau, Nature **530**, 194 (2016).
[13] D. Dreon, L. Sidorenkov, C. Bouazza, W. Maineult, J. Dalibard, and S. Nascimbène, J. Phys. B **50**, 065005 (2017).
[14] E. Lucioni, G. Masella, A. Fregosi, C. Gabbanini, S. Gozzini, A. Fioretti, L. Del Bino, J. Catani, G. Modugno, and M. Inguscio, Eur. Phys. J. Special Topics **226**, 2775 (2017).
[15] J. Ulitzsch, D. Babik, R. Roell, and M. Weitz, Phys. Rev. A **95**, 043614 (2017).
[16] J. Becher, S. Baier, K. Aikawa, M. Lepers, J.-F. Wyart, O. Dulieu, and F. Ferlaino, Phys. Rev. A **97**, 012509 (2018).
[17] P. Ilzhöfer, G. Durastante, A. Patscheider, A. Trautmann, M. Mark, and F. Ferlaino, Phys. Rev. A **97**, 023633 (2018).
[18] C. Ravensbergen, V. Corre, E. Soave, M. Kreyer, S. Tzanova, E. Kirilov, and R. Grimm, arXiv preprint arXiv:1801.05658 (2018).
[19] A. Stone, *The Theory of Intermolecular Forces* (Oxford University Press, New York, 1996).
[20] M. Lepers and O. Dulieu, in *Cold Chemistry: Molecular Scattering and Reactivity Near Absolute Zero*, edited by O. Dulieu and A. Osterwalder (Royal Society of Chemistry, London, 2017) Chap. 4, pp. 150–202.
[21] M. Baranov, Phys. Rep. **464**, 71 (2008).
[22] T. Lahaye, C. Menotti, L. Santos, M. Lewenstein, and T. Pfau, Rep. Prog. Phys. **72**, 126401 (2009).
[23] M. Baranov, M. Dalmonte, G. Pupillo, and P. Zoller, Chem. Rev. **112**, 5012 (2012).
[24] P. Żuchowski, J. Aldegunde, and J. Hutson, Phys. Rev. Lett. **105**, 153201 (2010).
[25] B. Pasquiou, A. Bayerle, S. Tzanova, S. Stellmer, J. Szczepkowski, M. Parigger, R. Grimm, and F. Schreck, Phys. Rev. A **88**, 023601 (2013).
[26] J. Barry, D. McCarron, E. Norrgard, M. Steinecker, and D. DeMille, Nature **512**, 286 (2014).
[27] A. Khramov, A. Hansen, W. Dowd, R. Roy, C. Makrides, A. Petrov, S. Kotochigova, and S. Gupta, Phys. Rev. Lett. **112**, 033201 (2014).
[28] M. Tomza, R. González-Férez, C. Koch, and R. Moszynski, Phys. Rev. Lett. **112**, 113201 (2014).
[29] P. Żuchowski, R. Guérout, and O. Dulieu, Phys. Rev. A **90**, 012507 (2014).
[30] M. Karra, K. Sharma, B. Friedrich, S. Kais, and D. Herschbach, J. Chem. Phys. **144**, 094301 (2016).
[31] G. Quéméner and J. Bohn, Phys. Rev. A **93**, 012704 (2016).
[32] D. Reens, H. Wu, T. Langen, and J. Ye, Phys. Rev. A **96**, 063420 (2017).
[33] T. Rvachov, H. Son, A. Sommer, S. Ebadi, J. Park, M. Zwierlein, W. Ketterle, and A. Jamison, Phys. Rev. Lett. **119**, 143001 (2017).
[34] D. Budker, D. DeMille, E. D. Commins, and M. S. Zolotorev, Phys. Rev. Lett. **70**, 3019 (1993).
[35] D. Budker, D. DeMille, E. Commins, and M. Zolotorev, Phys. Rev. A **50**, 132 (1994).
[36] A. Cingöz, A. Lapierre, A.-T. Nguyen, N. Leefer, D. Budker, S. Lamoreaux, and J. Torgerson, Phys. Rev. Lett. **98**, 040801 (2007).
[37] N. Leefer, C. Weber, A. Cingöz, J. Torgerson, and D. Budker, Phys. Rev. Lett. **111**, 060801 (2013).
[38] B. Roberts, Y. Stadnik, V. Dzuba, V. Flambaum, N. Leefer, and D. Budker, Phys. Rev. D **90**, 096005 (2014).
[39] K. Van Tilburg, N. Leefer, L. Bougas, and D. Budker, Phys. Rev. Lett. **115**, 011802 (2015).
[40] N. Leefer, A. Gerhardus, D. Budker, V. Flambaum, and Y. Stadnik, Phys. Rev. Lett. **117**, 271601 (2016).

[41] J.-F. Wyart, Physica **75**, 371 (1974).

[42] A. Kramida, Yu. Ralchenko, J. Reader, and and NIST ASD Team, NIST Atomic Spectra Database (ver. 5.3), [Online]. Available: `http://physics.nist.gov/asd` [2016, March 8]. National Institute of Standards and Technology, Gaithersburg, MD. (2015).

[43] K.-K. Ni, S. Ospelkaus, D. Wang, G. Quéméner, B. Neyenhuis, M. De Miranda, J. Bohn, J. Ye, and D. Jin, Nature **464**, 1324 (2010).

[44] D. Varshalovich, A. Moskalev, and V. Khersonskii, *Quantum theory of angular momentum* (World Scientific, 1988).

[45] M. Lepers, J.-F. Wyart, and O. Dulieu, Phys. Rev. A **89**, 022505 (2014).

[46] M. Lepers, Y. Hong, J.-F. Wyart, and O. Dulieu, Phys. Rev. A **93**, 011401R (2016).

[47] H. Li, J.-F. Wyart, O. Dulieu, S. Nascimbène, and M. Lepers, J. Phys. B **50**, 014005 (2017).

[48] H. Li, J.-F. Wyart, O. Dulieu, and M. Lepers, Phys. Rev. A **95**, 062508 (2017).

[49] R. Cowan, *The theory of atomic structure and spectra*, 3 (Univ of California Press, 1981).

[50] J.-F. Wyart, private communication (2018).

[51] This value is arbitrary, as there is no experimental Einstein coefficient between levels of [Xe]$4f^{10}5d6s$ and [Xe]$4f^{10}6s6p$ configurations.

[52] V. Dzuba, V. Flambaum, and M. Kozlov, Phys. Rev. A **50**, 3812 (1994).

[53] E. Eliel, W. Hogervorst, G. Zaal, K. van Leeuwen, and J. Blok, J. Phys. B **13**, 2195 (1980).

[54] P. Julienne, T. Hanna, and Z. Idziaszek, Phys. Chem. Chem. Phys. **13**, 19114 (2011).

[55] E. Den Hartog, L. Wiese, and J. Lawler, J. Opt. Soc. Am. B **16**, 2278 (1999).